7

Quantitative myocardial perfusion with dynamic contrast-enhanced imaging in MRI and CT theoretical models and current implementation

Gert Jan Pelgrim
Astri Handayani
Hildebrand Dijkstra
Niek H.J. Prakken
Riemer H.J.A. Slart
Matthijs Oudkerk
Peter M.A. van Ooijen
Rozemarijn Vliegenthart
Paul E. Sijens

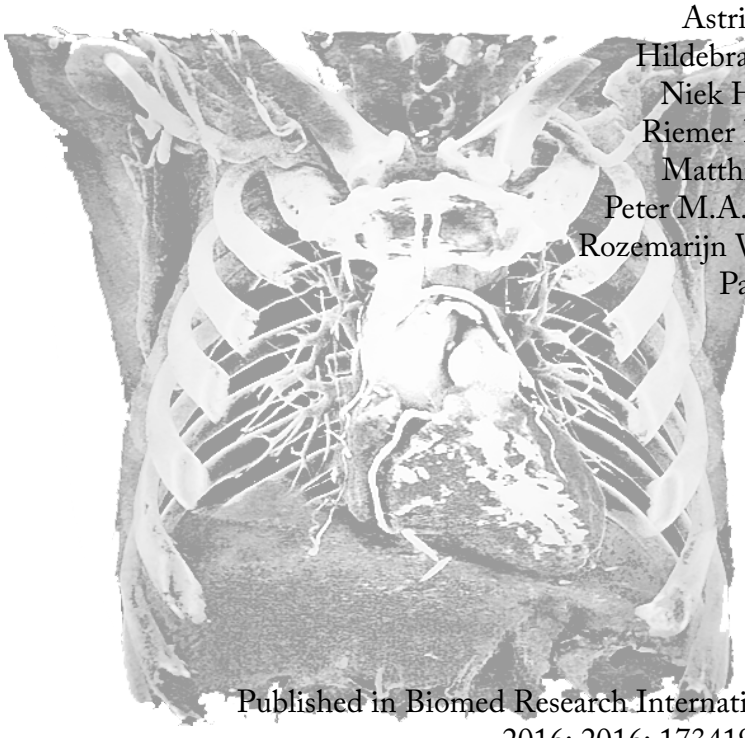

Published in Biomed Research International (2016)
2016; 2016; 1734190; 12 pages

507555-L-bw-Pelgrim
Processed on: 26-1-2017

Abstract

Technological advances in magnetic resonance imaging (MRI) and computed tomography (CT), including higher spatial and temporal resolution, have made possible the prospect of performing absolute myocardial perfusion quantification, previously only achievable with positron emission tomography (PET). This could facilitate integration of myocardial perfusion biomarkers into the current workup for coronary artery disease (CAD), as MRI and CT systems are more widely available than PET scanners. Cardiac PET scanning remains expensive and is restricted by the requirement of a nearby cyclotron. Clinical evidence is needed to demonstrate that MRI and CT have similar accuracy for myocardial perfusion quantification as PET. However, lack of standardization of acquisition protocols and tracer kinetic model selection complicates comparison between different studies and modalities. The aim of this overview is to provide insight into the different tracer kinetic models for quantitative myocardial perfusion analysis, and to address typical implementation issues in MRI and CT. We compare different models based on their theoretical derivations and present the respective consequences for MRI and CT acquisition parameters, highlighting the interplay between tracer kinetic modeling and acquisition settings.

Introduction

Myocardial perfusion imaging (MPI) is commonly used to investigate myocardial ischemia. While different modalities for MPI have different diagnostic accuracy, the overall accuracy to diagnose hemodynamically significant coronary artery disease (CAD) is good (1). Analysis of MPI results in the clinical setting is mostly performed by visual evaluation of presence and pattern of hypoenhancement of the myocardium during first pass of intravenously injected contrast. Presence of regions with normal perfusion is essential for this method to work. This is a limitation for diagnosis of patients with multi-vessel disease or balanced ischemia (2). MPI can only distinguish multi-vessel disease and balanced ischaemia when quantitative measures of myocardial perfusion are provided.

Positron emission tomography (PET) was the first technique to establish quantitative measures for perfusion. In PET, time-resolved acquisition of the first-pass of tracer uptake and direct quantification of tracer concentration were developed. With those parameters quantified, tracer kinetic modeling (1-compartment or 2-compartment modeling) could be applied to produce independent estimates of perfusion in stress and rest, known as absolute perfusion measurement (ml/g/min). This technique has been validated using microsphere comparison (2-4). Furthermore, added clinical value beyond relative and visual perfusion analysis has been demonstrated (5-8). The myocardial perfusion reserve (MPR), calculated from PET-derived perfusion measurement at stress and rest, was shown to be an important predictor of cardiovascular events (9-11).

A limitation of cardiac PET is the relatively high cost and the need for an on-site cyclotron, depending on the tracer. Recent developments with the new 18F-tracer flurpiridaz or other improved tracers could obviate the need for an on-site cyclotron. Flurpiridaz has shown good linearity of myocardial uptake with perfusion at a large flow range, excellent myocardial retention, low background noise in adjacent organs, and a relatively long half-life (110 min) (12).

Magnetic resonance imaging (MRI) and computed tomography (CT) imaging could be important modalities to compete with PET for the complete workup of cardiac patients. Recent developments have sparked interest for myocardial perfusion quantification using these techniques. State-of-the-art MRI and CT have better spatial and temporal resolution compared to PET. Integration of MRI and CT into current workup for coronary artery disease (CAD) also profits from their wider availability, lower costs and increasing clinical role in comprehensive diagnosis of CAD. The validity and non-inferiority of MRI and CT compared to PET measurements need to be demonstrated before a decision regarding the preference for MRI or CT over PET for myocardial perfusion quantification can be reached. Lack of standardized acquisition and modeling protocols for myocardial perfusion acquisition have complicated comparison between studies and modalities.

The aim of this study is to provide insight into the tracer kinetic models in absolute myocardial perfusion quantification, and their implementation requirements for CT and MRI. A further aim was to analyze the factors that influence myocardial perfusion quantification.

Myocardial perfusion imaging in MRI and CT

Perfusion refers to the delivery of blood to the tissue via the intravascular capillary pathway. Perfusion imaging uses dynamic contrast-enhanced acquisition to observe the first-pass dynamics of contrast agent delivery into the tissue of interest over time. For myocardial perfusion quantification, the first-pass contrast dynamics at the respective supplying artery or other arterial input sites should be captured as well. The typical arterial input sites for myocardial perfusion are the left ventricular cavity in MRI or the descending aorta in CT.

Contrast agent

MRI and CT use different agents (gadolinium and non-ionic iodine, respectively) to acquire contrast in the myocardial perfusion scans: both small molecules <1kDa, typical particle diameters of 0.82 nm for gadolinium dimeglumine and 1.4 nm of iohexol) that distribute to the interstitial space and generally do not enter the intracellular space. Actually, MRI contrast agents do interact with the intracellular space by changing the relaxivity of water that diffuses freely into the cell. The diffusion constants for MRI and CT contrast-agents are roughly similar: 2.7 x 10-2 m^2/s for gadolinium dimeglumine, and 2.5 x 10-2 m^2/s for iohexol (13, 14). Although the non-ionic iodine contrast agents typically have a much higher viscosity compared to gadolinium, neither CT nor MRI contrast agents have significant effects on the viscosity of the blood stream (15, 16). Gadolinium-based contrast-agents have limited linearity of contrast enhancement to contrast concentration, with higher dose resulting in blood signal saturation (17, 18). A typical dose of gadolinium contrast for visual and quantitative analysis is 0.05 mmol/kg at an injection rate of 4-5 ml/s. Dosages as low as 0.03 mmol/kg body weight have been recommended to prevent contrast saturation both in the myocardium and in the arterial input function (19). Iodine-based contrast agents on the other hand have more straightforward and steady linearity of contrast enhancement to contrast concentration, which greatly simplifies absolute quantification (20). In myocardial perfusion studies with multi-detector CT, iodine contrast agents are administered at an injection rate of 3-5 ml/s and a volume of 60-70 ml (21, 22). The resulting lengthy administration of CT contrast (longer than the first pass of diffusion), however, violates the principles of indicator dilutor theory and will affect the accuracy of quantification.

Acquisition of myocardial perfusion imaging

In MRI, myocardial perfusion imaging is mainly based on T1-weighted pulse sequences, where interactions of paramagnetic gadolinium (Gd3+) with surrounding water molecules result in lower T1 relaxation times of the protons involved, resulting in signal enhancement showing as hyperintensity on the T1-weighted image, reflecting the distribution of gadolinium (23). The current protocol allows acquisition of three myocardial short-axis slices at every heart beat with a typical spatial resolution of 1.5 x 1.5 x 10 mm^3, performed during 50-60 consecutive heart beats. In dynamic contrast enhanced MRI, temporal resolution generally is in the order of 1 sec (1-2 cardiac cycles). Recently introduced advanced accelerated imaging sequences achieve whole heart 3-D perfusion MRI with a voxel resolution of 2.3 x 2.3 x 5 mm^3, although with their reduced temporal resolution not a substitute for quantitative estimation of myocardial blood flow (24). In CT, with dynamic shuttling mode acquisition, whole heart coverage with higher spatial resolution can be obtained (0.3 x 0.3 x 5 mm^3) at every 2-3 heart beats (22). In contrast, CT scanners with wider detectors, of up to 16 cm, can achieve whole heart acquisition in a single heartbeat (25). In both methods, perfusion imaging is performed over 20-30 consecutive heart beats. CT has a high temporal resolution. The latest generation of dual-source CT scanners has a temporal resolution per acquisition of approximately 63 ms. However, dual-source CT scanners need to shuttle between two positions, resulting in a time interval in-between scans of once every second heart beat and, for high heart rhythms, once every three cardiac cycles. The 256- and 320-slice CT scanners have lower temporal resolution per acquisition (in the order of 135 ms), but these scanners do not have to shuttle between two positions in order to acquire information about the whole heart, providing the opportunity to image at every heartbeat (at the cost of higher dose). A limitation in CT, and especially also in dynamic CT perfusion studies, is that the radiation dose is directly related to the number of images acquired. For a thorough overview of CT perfusion acquisition techniques one is referred to the review of Rossi et al (26).

Why use modeling in MRI and CT

In theory, tissue perfusion can be inferred from the apparent contrast enhancement without any complex modeling, assuming that the contrast agent is hemodynamically inert. This hypothesis holds true if two criteria are met with: 1) a linear relationship between contrast enhancement and contrast concentration (*ex vivo* linearity) and 2) a linear relationship between apparent contrast enhancement and perfusion (*in vivo*/uptake linearity).

Ex vivo linearity is present in PET tracers as well as in CT iodine-based contrast agents regardless of their concentrations and, and in MR gadolinium only up to a certain concentration limit (17, 18). *In vivo*/uptake linearity is limited in case of extravasating contrast agent. Most contrast agents in perfusion imaging do not only flow to the intravascular space, but also distribute to the extracellular

extravascular space (EES). Only in case EES extraction fraction is constant within the range of physiological perfusion flow, the apparent contrast enhancement will be linear to perfusion, as is the case with ^{15}O-water and ^{18}F-flurpiridaz in PET. However, in most tracers such as ^{13}N-ammonia (12, 23, 27), 82Rb-Rubidium (12, 23), gadolinium (23, 28-30) and iodine(23, 31, 32), the extraction fractions decrease non-linearly with increasing perfusion, causing reduced *in vivo*/uptake linearity.

To correct for the effect of these extravasating tracers or contrast agents on contrast enhancement, tracer kinetic modeling attempts to separate the dynamics of contrast agent in the intravascular space and the EES over time to yield more accurate perfusion estimation. These modeling techniques have been successfully applied in PET myocardial perfusion imaging with different tracers, including ^{13}N-ammonia and ^{82}Rb-rubidium (33). It is theoretically feasible to implement the same principles in MRI and CT, using tracer kinetic modeling.

Tracer Kinetic modeling

Tracer kinetic modeling essentially relates the dynamics of tracer or contrast agent concentration in tissue (myocardium) to that in the supplying artery referred to as arterial input function (AIF). The contrast dynamics over time are obtained by tracing the myocardium and AIF voxels from the dynamic contrast-enhanced acquisition (*figure 1*).

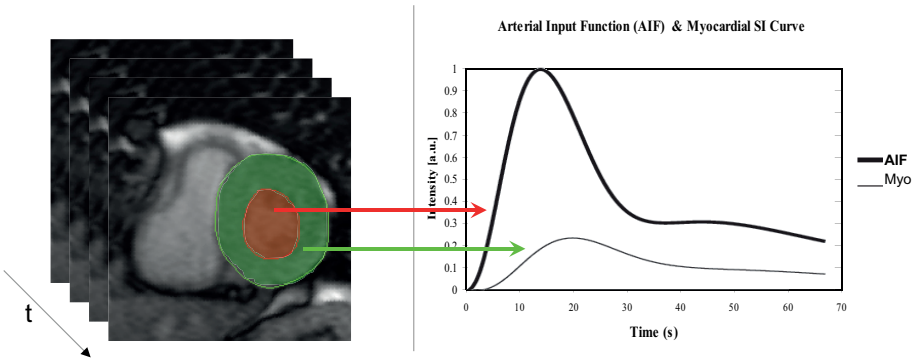

Figure 1: *Myocardial (green voxels) and arterial input function (red voxels) tracing to produce contrast dynamics time curves.*

The mathematical relation between contrast dynamics in the tissue and in the AIF is represented by an impulse response function (IRF) (*figure 2*). As a result of a one unit-amplitude of an infinitely narrow input bolus (impulse bolus) in the arterial inlet (*figure 2a*), contrast retention will occur in the tissue with a certain dynamic proportion in time, defined as IRF (*figure 2b*). In a perfusion imaging study, the AIF can be considered as a train of time-shifted and magnitude-scaled impulse boluses (*figure 2c*) producing a corresponding train of time-shifted

and magnitude-scaled IRFs in the tissue (*figure 2d*). An iterative curve-fitting operation called deconvolution can then be applied to reconstruct the IRF from the AIF and tissue enhancement curves. Since deconvolution may lead to more than one mathematically suitable solution, it is necessary to restrict the operation by requiring the IRF to follow a certain parameterized formulation specific for each perfusion model. Therefore, perfusion flow is estimated from those IRF parameters providing the best fit at deconvolution.

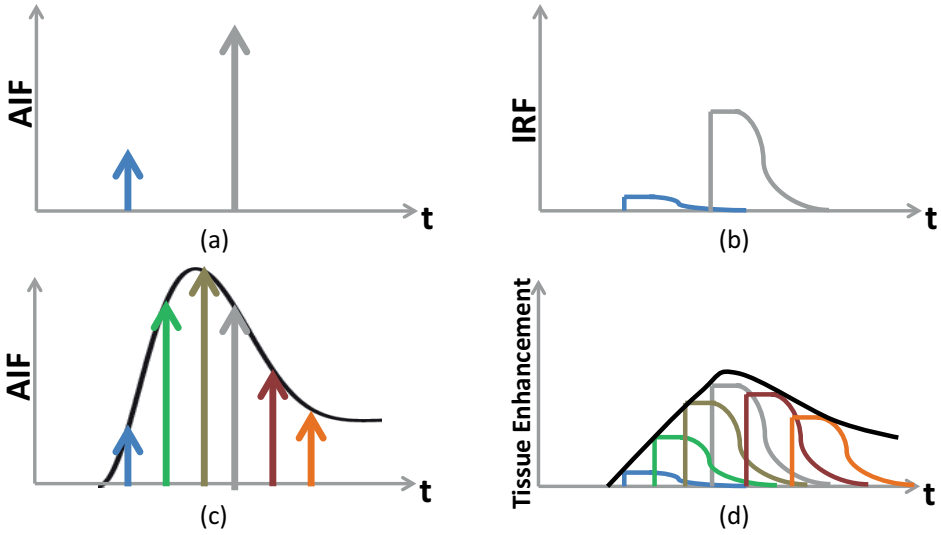

Figure 2: *Single arterial inlets are shown with different magnitude scale in different time instance (panel A) and the respective magnitude-scaled impulse response function (IRF) in the tissue (panel B). A contrast bolus can be modeled as trains of arterial inlets (panel C), producing trains of magnitude-scaled IRF in the tissue (panel D). Deconvolution aims to reconstruct the IRF that fits the relation between the red and green lines in panel C and D, respectively.*

Different tracer kinetic models

Tracer kinetic models for absolute myocardial perfusion quantification can be classified into three model groups: distributed parameter, compartmental, and indicator dilution theory approaches, each of which has been developed into more specific models. For thorough explanation of the distributed parameter and compartmental models one is referred to the technical paper of Sourbron and Buckley and two manuscripts of Jerosch-Herold for the indicator dilution theory approach (34-36). In the present overview those modeling approaches are solely compared on the basis of physical interpretation of their respective IRF.

For extravasating contrast agents as used in MRI and CT, contrast agent molecules distribute across two spaces, i.e., the intravascular space and the EES (*figure 3*). Each space is defined by volume, rate, and transit time parameters. The relative intravascular plasma space is defined as the intravascular plasma volume relative divided by total tissue volume (Vp). The intravascular flow rate (F) equals the

blood perfusion rate per unit of volume of tissue and the mean capillary transit time (MTTc) is the ratio between the blood volume and the tissue blood perfusion rate. Similarly, the tissue interstitial volume (Ve) is the sum of extravascular and extracellular volume (EES) contained in a volume of tissue. The two-way exchange rate to and from the EES is called the permeability-surface product, PS, and the MTTe is the mean transit time for the EES. Additionally, an extraction fraction (E) describes the proportion of the contrast agent distributing to the EES. IRF is affected by the inflow of contrast (perfusion), two-way exchange of contrast between plasma and the EES, extraction fraction, and permeability. High order perfusion models take into account such dynamics as completely as possible, although assumptions remain and additional variables do not necessarily yield more accurate results. The lower order models assume some parameters or dynamics to be negligible compared to others, thus simplifying the model. In *figure 4* each modeling approach is illustrated, with the formulation presented in *table 1*.

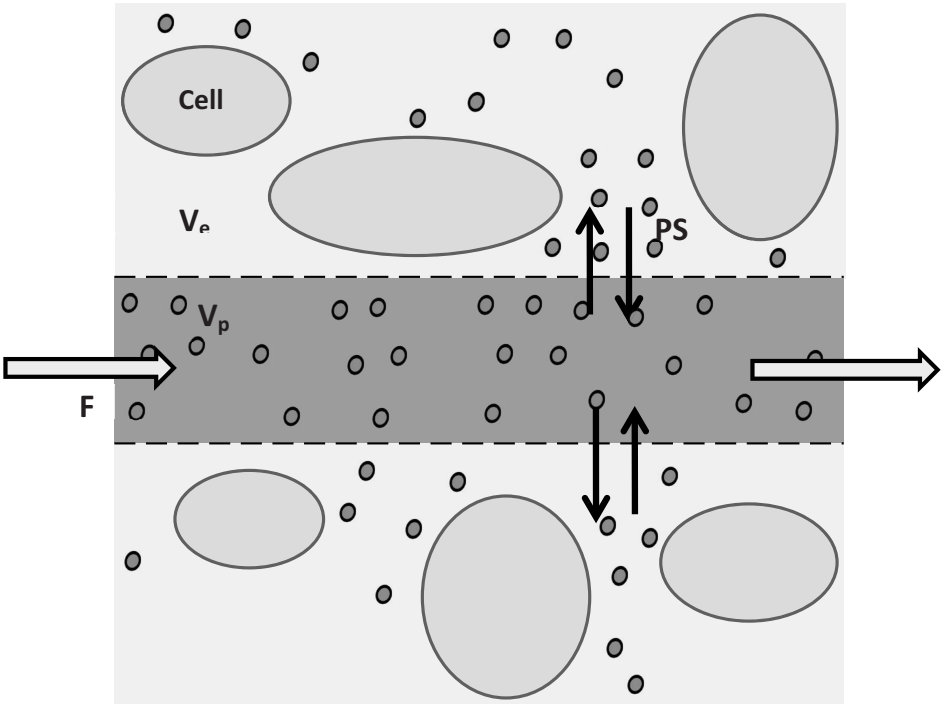

Figure 3: *Illustration of contrast agent (blue dots) distribution in the tissue: vp is the plasma volume within the intravascular space, ve is the extravascular extracellular space, F is the perfusion flow within the intravascular space, PS is the permeability surface exchange rate between Vp and Ve. Another parameter, the extraction fraction (E) denotes the proportion of contrast agent exchanged to the extravascular extracellular space.*

Models based on axially distributed parameters

Distributed parameter model

This model takes into account the most detailed aspects of contrast dynamics at the tissue level. It assumes contrast concentration within the intravascular space and EES to be varying temporally and axially along the longitudinal direction of the perfusion flow (*figure 4a*). As such, the model is able to estimate every volume, rate, and time parameter specified in the intravascular and the interstitial space, as well as the extraction fraction. The distributed parameter model has been applied to estimate MRI stress/rest myocardial perfusion in healthy volunteers (37).

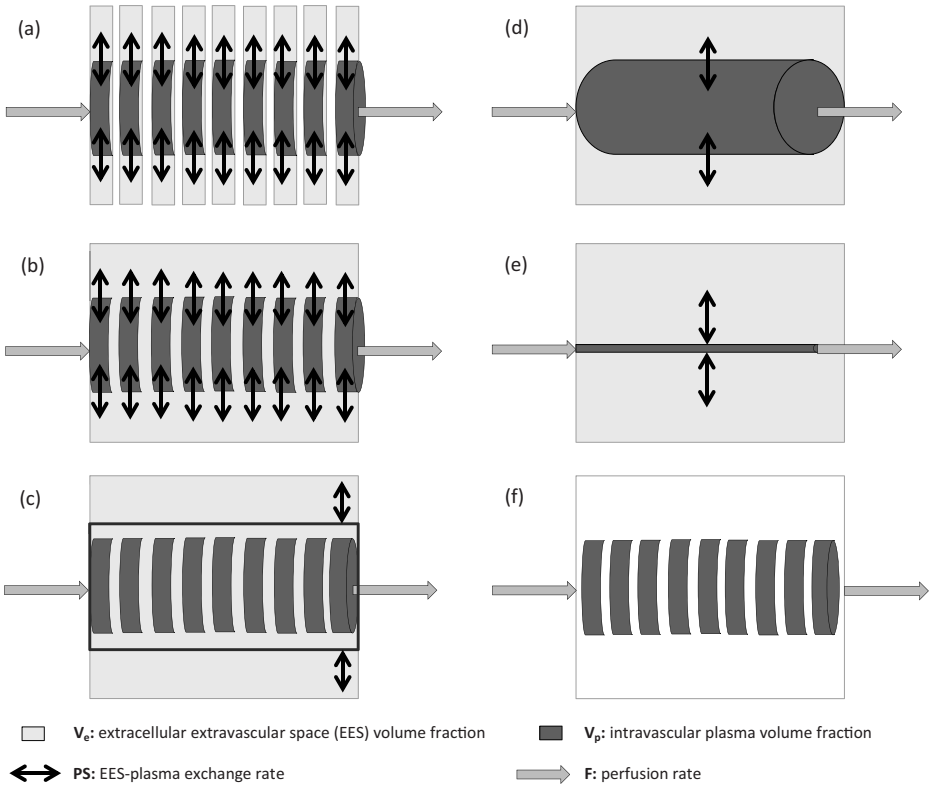

Figure 4: *Schematic representation of different tracer kinetic models: (a) distributed parameter model, (b) tissue homogeneity model, (c) adiabatic approximation of tissue homogeneity model, (d) 2-compartments model, (e) 1-compartment (Toft's) model, (f) Fermi model.*

Table 1: *Tracer kinetic model formulation*

Model	Output Parameters	Impulse Response Function (IRF)
Distributed Parameter	F, PS, MTT_c, MTT_e, v_p, v_e	not available in time domain
Tissue Homogeneity	F, E, MTT_c, v_p, v_e	
Adiabatic Approximation of Tissue Homogeneity	F, E, MTT_c, v_p, v_e (assuming $v_p << v_e$)	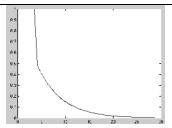 $IRF(t) = \begin{cases} F, 0 < t \le \frac{F}{vp} \\ EF \exp^{-\frac{EF}{ve}(t)}, t > \frac{F}{vp} \end{cases}$
2-compartments	F, PS, v_p, v_e	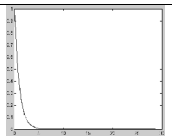 $IRF(t) = F \exp^{-\frac{F}{vp}(t)} + PS \exp^{-\frac{PS}{ve}(t)}$
1-compartment (Extended Toft's)	K_{trans}, v_p, v_e	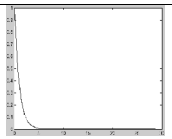 $IRF(t) = Ktrans \exp^{-\frac{Ktrans}{ve}(t)} + vp\partial(t)$
1-compartment (Toft's)	K_{trans}, v_e (assuming $v_p << v_e$)	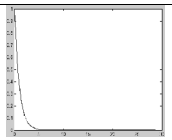 $IRF(t) = Ktrans \exp^{-\frac{Ktrans}{ve}(t)}$
Fermi	F, MTT_c, k (in extravasating contrast agent, only F is of physiological value)	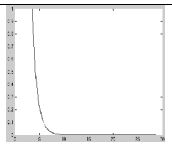 $IRF(t) = \frac{F}{\exp^{k(t-MTTc)}+1}$
Model-independent deconvolution	F (estimated as initial IRF magnitude)	no specific formulation

F: perfusion rate, PS: extracallular extravascular space (EES) exchange rate, MTT_c: capillary mean transit time, MTT_e: EES mean transit time, v_p : EES volume fraction, v_e: intravascular plasma volume fraction, K_{trans}: compound transfer constant (perfusion & EES exchange), k: venous clearance rate for intravascular contrast agent

Tissue homogeneity model

This model by Johnson and Wilson assumes that the contrast concentration only varies longitudinally in the intravascular space and not in the EES (*figure 4b*) (38). With this assumption, the model loses the ability to estimate the time parameter of the EES (MTTe) but can still estimate the other intravascular and EES parameters. These two axially-distributed models require special numerical treatments for model fitting, (i.e. multiple or Laplace-domain fitting) due to their complexity (39, 40).

Adiabatic approximation of tissue homogeneity model

Developed by Lawrence and Lee, this model further simplifies the tissue homogeneity model by assuming that the contrast exchange between the intravascular space and the EES only takes place in the venous outlet (41). Therefore, the rate of concentration change in the EES is much slower than in the intravascular space (*figure 4c*). Adiabatic model fitting can be performed as a standard time-domain deconvolution with IRF, as specified in Table 1: height and length of the plateau correspond to perfusion flow and capillary mean transit time (MTTc), respectively, while the decay rate of the mono-exponential function represents the venous clearance. This model was first proposed in brain studies, but has been used in oncological and cardiac studies afterwards (42-46).

Implementation issues

The main limitations for axially-distributed models are 1) the need of a fast acquisition rate to support MTTc estimation, and 2) the more complicated and noise-sensitive fitting methods. Faster perfusion produces shorter MTTc, requiring more compact contrast bolus to accurately capture the MTTc from the contrast dynamics.

Models based on compartments

The main difference between the compartmental and axially-distributed model lies in the assumption that intravascular and EES contrast agent concentrations only vary with time, and not axially (*figure 4d-e*). Because the axial contrast concentration gradient is considered negligible, transit time cannot be estimated, limiting the modeling results to the volume and rate parameters.

2-compartmental and 1-compartmental model

The typical IRF of a 2-compartment model takes the shape of a bi-exponential function, without an initial plateau for the capillary inflow phase due to the absence of transit time estimation. The faster-decaying exponential refers to the transfer towards the EES while the slower exponential refers to the transfer from the EES. On the other hand, the IRF of a 1-compartment model takes the shape of a mono-exponential function. The maximum magnitude of the IRF corresponds to

Ktrans, a compound tissue transfer constant formulated by multiplying perfusion (F) by the contrast extraction fraction (E) (47). Three main 1-compartmental models are distinguished.

Toft s Models

The basic Toft s model refers specifically to immediate and complete tracer extraction fraction (E=1) and negligible Vp compared to, such that Ktrans represents perfusion flow (47). Since Vp is not negligible in the myocardium, one study applied an Extended Toft s model where Vp is added to the original IRF (47, 48). However, it has been argued that under the Extended Toft s model, Ktrans is closer to the EES exchange rate than to the perfusion flow (49).

Patlak model

The Patlak model includes only data portions from the early phase of contrast arrival, when the contrast agent has not significantly filled the EES yet. Here, EES contrast concentration is not adequate to cause diffusion of contrast molecules back to the intravascular space. Under this assumption, Ve and Vp can be considered a single compartment with a single transfer rate (Ktrans) (50). The temporal growth in the EES contrast concentration will be linear to the rate of contrast transfer to the EES (Ktrans) and the AIF contrast concentration. Therefore, Ktrans of the Patlak model can be reconstructed from the slope of a correlation map between tissue contrast concentration and the area under the curve of the AIF. However, care should be taken to make sure that only appropriate data portions are used. The Patlak model has been used in human MRI studies of myocardial perfusion, with an acquisition rate matching every heartbeat, as well as in animals with the acquisition rate matching every other heartbeat (30, 48, 51).

Maximum slope method

The maximum slope method is derived from exactly the same assumptions as the Patlak model, therefore requiring the same portion of data points and suffering the same concerns. The Patlak-equivalent Ktrans is derived by normalizing the maximum slope of the tissue concentration to the maximum (peak) concentration of the AIF. The tissue maximal upslope is calculated by linear fitting while the AIF peak is derived from gamma-variate fitting. The method has been implemented in an older study based on electron-beam CT as well as in more recent myocardial perfusion studies with dual-source CT (21, 52-54).

Implementation issues

The main critique on the 1-compartment model is that Ktrans is a multiplication of extraction fraction (E) and perfusion instead of a sole perfusion (F) indicator. Limited number of MRI studies have shown a non-linearly decreasing extraction suggesting a limited range of Ktrans proportionality with perfusion if this parameter is to be derived from gadolinium (18, 28-30). Correcting Ktrans for the

extraction fraction (E) improved the correlation between Patlak-derived Ktrans and microsphere perfusion in an animal experiment (62).

Models based on Indicator Dilution Theory

The Fermi model

The Fermi model was initially developed for studies with a purely intravascular indicator. Assuming an axially-varying contrast concentration in the intravascular space, it was observed that the IRF of an intravascular indicator resembled the shape of the Fermi function (55). The amplitude, width of initial plateau and subsequent curve decay rate of the fitted Fermi function represents perfusion, capillary mean transit time, and venous clearance rate, respectively (Table 1). For extravasating tracers, the validity of the Fermi model holds as long as the tracer concentration in the EES is substantially lower than in the intravascular space ($c_e << c_p$), a condition assumed to be attainable in the first-pass of tracer circulation (36). The Fermi model has been used in many MR human and animal studies (2, 36, 56-60). and it has been used in one CT porcine study (32).

Model-independent deconvolution

The previous perfusion models have been driven by specific physical assumptions on the distribution of contrast agent in the tissue, culminating into exact IRF formulation. A model-independent approach attempts to overcome these tissue-specific assumption problems by applying more generic mathematical constraints in the IRF calculation. With the central-volume principle applied in the indicator dilution theory, the initial magnitude of the IRF is then assumed as perfusion regardless of the shape of the IRF (35). Studies with high data quality have shown excellent agreement of model-independent deconvolution with true perfusion (simulation study) and microspheres (porcine study, n=3), as well as with PET in healthy volunteers (n=5) (35, 61).

Implementation issues

Since the indicator dilution approach does not presume any separation between the intravascular and the EES contrast dynamics, its perfusion estimation is uncorrected for EES exchange. Therefore, the same concern as in 1-compartment models, i.e., the consistency of perfusion representation over the physiological range of perfusion, also applies to indicator dilution theory models.

Influence of different acquisition settings

In the previous paragraphs, the different perfusion models were discussed. Those models offer different degrees of perfusion evaluation. When more accurate quantification of perfusion is desired, consequently, more detailed information of contrast dynamics is required. This leads to more demanding acquisition settings (i.e., faster acquisition rate, higher contrast-to-noise ratio). As a result, more

detailed models will are more sensitive to noise, because a small change in the contrast dynamics will have more impact on the parameter estimations.

Key acquisition factors

Jerosch-Herold et al. performed a thorough review on specific MRI imaging requirements (19). Minimal requirements of several general key acquisition/ image quality parameters that influence the output of tracer kinetic models are listed here.

1) A compact contrast bolus is needed to ensure that the contrast dynamics contains information as requested by the modeling. An increasingly dispersed bolus is known to cause increasing perfusion underestimation and variability, especially at higher flow rate (62). As a rough guidance, the contrast bolus should be compact enough to accommodate a clear definition of the peak enhancement in the AIF as well as in the tissue (and even more compact in case of the use of the axially-distributed model). A gadolinium injection rate of at least 3 ml/s, and optimally 4 ml/s, has been recommended for MRI myocardial perfusion assessment (18, 63). More prominent bolus dispersion can be expected in CT due to the typically larger injected contrast volume.

2) In order to estimate the flow rate and transit time parameters, a sufficiently fast acquisition rate (temporal resolution) is needed to capture the fastest change described by the model. When only the flow rate parameter is analyzed, the minimum scan interval is determined by the time-to-peak (TTP) of the AIF. When both rate and transit time parameters are concerned, the mean capillary transit time (MTTc) determines the minimum scan interval. In other tissues a considerable underestimation was found when the temporal resolution was reduced, with both CT and MRI (62, 64-68).

(3). In order to estimate volume parameters, the acquisition period should be at least within the order of the transit time parameter of the concerned volume, to ensure proper capture of the arrival and clearance of contrast agent.

(4) In-plane spatial resolution should be adequate to prevent partial volume effects, especially if voxel-wise tracer kinetic modeling is to be applied. In the data acquisition this means that voxels are best small and isotropic (cubic rather than rectangular, etc.). This is hard to realize in MRI where the in-plane spatial resolution is approximately 5 times lower than in CT (1.5 x 1.5 mm^2 versus 0.3 x 0.3 mm^2) with slice thickness much larger than in-plane resolution. In post-processing, the quantification resolution particularly worsens due to partial volume effects in CT where investigators have typically analyzed the CT perfusion in slices thicker than the native resolution (5). Signal-to-noise ratio (SNR) concerns the total variability in the contrast dynamics. Small variations in contrast dynamics may influence the precision of tracer kinetic modeling. The use of higher Tesla machines in MRI may provide better SNR without compromising

spatio-temporal resolution, although inherent problems with RF homogeneity can adversely impact quantification. Implementation of higher tube current in CT can also improve SNR by reducing variability in contrast dynamics and the error in model fitting (19, 55). A disadvantage of higher tube current is the increase in radiation dose. A decrease in tube voltage could increase SNR, because of the K-edge of iodine, which lies around 35 kV. If possible, a lower tube voltage would be beneficial for contrast scans, and additionally lowers radiation dose (69).

Clinical implication and conclusion

Regarding the choice of model used, we suggest that one should use the simplest possible model that can explain the contrast dynamics. It is worth noting that the use of higher-order models will only be beneficial when the acquisition is optimized to capture the additional contrast dynamic details requested by the model. Considering the current imaging and contrast administration setup for MRI and CT myocardial perfusion imaging, the 1-compartmental and Fermi models seem to be the most technically applicable. Axially-distributed models require an acquisition rate at the order of MTTc and a sufficiently compact bolus to identify the capillary inflow phase. Balancing such demand with clinical requirements for spatial resolution and coverage could be problematic. Apart from optimal data quality, model-independent deconvolution also requires knowledge for selection of the regularization parameter, which may not be available in every imaging center.

Issues for clinical adoption go beyond the accuracy of the quantitative myocardial perfusion value itself. The assumptions made by each model are coupled with the theoretical pitfalls we have tried to identify in our appraisal. The major complication with quantitative MR perfusion is in the limited linearity of contrast enhancement to contrast concentration, requiring lower dose of gadolinium, thus compromising the accuracy of visual analysis as well as the precision of perfusion estimation. CT perfusion on the other hand greatly simplifies quantification efforts by offering a linear relationship between contrast enhancement and concentration. However, current CT imaging setup suffers reduced image quality due to the shuttling mode acquisition and limited temporal resolution as well as acquisition period due to the radiation dose constraint; both reduce the precision and accuracy of perfusion estimation.

Limited studies have mentioned instability issues of higher-order models. More investigations are required (37, 70). Reproducibility of perfusion values is highly related to the imaging quality, where specific issues such as acquisition/reconstruction artifacts need to be taken care for in both modalities before implementing the model.

An important issue for the clinical setting would be to establish the expected physiological variability across different subjects, so that the usability of quantitative myocardial perfusion in diagnostic or sequential observation setting can be verified. Quantitative PET studies for instance have shown considerable heterogeneity in myocardial perfusion of healthy volunteers, related to factors such as age, gender, rate-pressure product, and other hemodynamic factors (71, 72). Furthermore, in the presence of COPD and hypertension, the value of myocardial perfusion reserve has been shown to be impaired without regional myocardial ischemia (73-75). The spectrum of physiological variability in myocardial perfusion should also be investigated with MRI and CT if myocardial perfusion quantification is to be adopted in clinical practice.

Studies investigating the performance of quantitative MRI and CT myocardial perfusion imaging in detecting CAD have been conducted with different reference standards, i.e., stenosis diameter, either derived from quantitative CT or invasive coronary angiography, fractional flow reserve, or even visual analysis of SPECT myocardial perfusion. None of these reference parameters actually capture the same functional phenomenon as myocardial perfusion. The anatomical aspect of a stenosis does not describe its functional relevance, while fractional flow reserve, even though being a functional parameter, indicates the hemodynamics of the focal coronary lesion rather than its systemic effect on myocardial microcirculation. The quantitative relationship between myocardial perfusion and the above parameters, therefore, can expected to be affected by broader physiological variability, which may be better captured by quantitative analysis than by visual assessment. However, the superiority of quantitative myocardial perfusion over mere visual analysis for diagnosis of hemodynamically significant CAD still needs to be proven.

References

1. Jaarsma C, Leiner T, Bekkers SC, Crijns HJ, Wildberger JE, Nagel E, et al. Diagnostic performance of noninvasive myocardial perfusion imaging using single-photon emission computed tomography, cardiac magnetic resonance, and positron emission tomography imaging for the detection of obstructive coronary artery disease: a meta-analysis. J Am Coll Cardiol. 2012 May 8;59(19):1719-28.

2. Morton G, Chiribiri A, Ishida M, Hussain ST, Schuster A, Indermuehle A, et al. Quantification of absolute myocardial perfusion in patients with coronary artery disease: comparison between cardiovascular magnetic resonance and positron emission tomography. J Am Coll Cardiol. 2012 Oct 16;60(16):1546-55.

3. Kuhle WG, Porenta G, Huang SC, Buxton D, Gambhir SS, Hansen H, et al. Quantification of regional myocardial blood flow using 13N-ammonia and reoriented dynamic positron emission tomographic imaging. Circulation. 1992 Sep;86(3):1004-17.

4. Choi Y, Huang SC, Hawkins RA, Kim JY, Kim BT, Hoh CK, et al. Quantification of myocardial blood flow using 13N-ammonia and PET: comparison of tracer models. J Nucl Med. 1999 Jun;40(6):1045-55.

5. Gewirtz H. PET measurement of adenosine stimulated absolute myocardial blood flow for physiological assessment of the coronary circulation. J Nucl Cardiol. 2012 Apr;19(2):347-54.

6. Kajander SA, Joutsiniemi E, Saraste M, Pietila M, Ukkonen H, Saraste A, et al. Clinical value of absolute quantification of myocardial perfusion with (15)O-water in coronary artery disease. Circ Cardiovasc Imaging. 2011 Nov;4(6):678-84.

7. Di Carli MF, Dorbala S, Meserve J, El Fakhri G, Sitek A, Moore SC. Clinical myocardial perfusion PET/CT. J Nucl Med. 2007 May;48(5):783-93.

8. Schindler TH, Schelbert HR, Quercioli A, Dilsizian V. Cardiac PET imaging for the detection and monitoring of coronary artery disease and microvascular health. JACC Cardiovasc Imaging. 2010 Jun;3(6):623-40.

9. Slart RH, Zeebregts CJ, Hillege HL, de Sutter J, Dierckx RA, van Veldhuisen DJ, et al. Myocardial perfusion reserve after a PET-driven revascularization procedure: a strong prognostic factor. J Nucl Med. 2011 Jun;52(6):873-9.

10. Tio RA, Dabeshlim A, Siebelink HM, de Sutter J, Hillege HL, Zeebregts CJ, et al. Comparison between the prognostic value of left ventricular function and myocardial perfusion reserve in patients with ischemic heart disease. J Nucl Med. 2009 Feb;50(2):214-9.

11. Juarez-Orozco LE, Glauche J, Alexanderson E, Zeebregts CJ, Boersma HH, Glaudemans AW, et al. Myocardial perfusion reserve in spared myocardium: correlation with infarct size and left ventricular ejection fraction. Eur J Nucl Med Mol Imaging. 2013 Aug;40(8):1148-54.

12. Maddahi J. Properties of an ideal PET perfusion tracer: new PET tracer cases and data. J Nucl Cardiol. 2012 Feb;19 Suppl 1:S30-7.

13. Gordon MJ, Chu KC, Margaritis A, Martin AJ, Ethier CR, Rutt BK. Measurement of Gd-DTPA diffusion through PVA hydrogel using a novel magnetic resonance imaging method. Biotechnol Bioeng. 1999 Nov 20;65(4):459-67.

14. Nair N, Kim WJ, Braatz RD, Strano MS. Dynamics of surfactant-suspended single-walled carbon nanotubes in a centrifugal field. Langmuir. 2008 Mar 4;24(5):1790-5.

15. Irace C, Tamburrini S, Bertucci B, De Franceschi MS, Gnasso A. Effects of iodinated contrast media on common carotid and brachial artery blood flow and wall shear stress. Eur Radiol. 2006 Dec;16(12):2721-7.

16. Reinhart WH, Pleisch B, Harris LG, Lutolf M. Influence of contrast media (iopromide, ioxaglate, gadolinium-DOTA) on blood viscosity, erythrocyte morphology and platelet function. Clin Hemorheol Microcirc. 2005;32(3):227-39.

17. Utz W, Niendorf T, Wassmuth R, Messroghli D, Dietz R, Schulz-Menger J. Contrast-dose relation in first-pass myocardial MR perfusion imaging. J Magn Reson Imaging. 2007 Jun;25(6):1131-5.

18. Ishida M, Sakuma H, Murashima S, Nishida J, Senga M, Kobayasi S, et al. Absolute blood contrast concentration and blood signal saturation on myocardial perfusion MRI: estimation from CT data. J Magn Reson Imaging. 2009 Jan;29(1):205-10.

19. Jerosch-Herold M. Quantification of myocardial perfusion by cardiovascular magnetic resonance. J Cardiovasc Magn Reson. 2010 Oct 8;12:57,429X-12-57.

20. O'Connor JP, Tofts PS, Miles KA, Parkes LM, Thompson G, Jackson A. Dynamic contrast-enhanced imaging techniques: CT and MRI. Br J Radiol. 2011 Dec;84 Spec No 2:S112-20.

21. Bamberg F, Hinkel R, Marcus RP, Baloch E, Hildebrandt K, Schwarz F, et al. Feasibility of dynamic CT-based adenosine stress myocardial perfusion imaging to detect and differentiate ischemic and infarcted myocardium in an large experimental porcine animal model. Int J Cardiovasc Imaging. 2014 Apr;30(4):803-12.

22. Bastarrika G, Ramos-Duran L, Schoepf UJ, Rosenblum MA, Abro JA, Brothers RL, et al. Adenosine-stress dynamic myocardial volume perfusion imaging with second generation dual-source computed tomography: Concepts and first experiences. J Cardiovasc Comput Tomogr. 2010 Mar-Apr;4(2):127-35.

23. Salerno M, Beller GA. Noninvasive assessment of myocardial perfusion. Circ Cardiovasc Imaging. 2009 Sep;2(5):412-24.

24. Jogiya R, Kozerke S, Morton G, De Silva K, Redwood S, Perera D, et al. Validation of dynamic 3-dimensional whole heart magnetic resonance myocardial perfusion imaging against fractional flow reserve for the detection of significant coronary artery disease. J Am Coll Cardiol. 2012 Aug 21;60(8):756-65.

25. Kikuchi Y, Oyama-Manabe N, Naya M, Manabe O, Tomiyama Y, Sasaki T, et al. Quantification of myocardial blood flow using dynamic 320-row multi-detector CT as compared with (1)(5)O-H(2)O PET. Eur Radiol. 2014 Jul;24(7):1547-56.

26. Rossi A, Merkus D, Klotz E, Mollet N, de Feyter PJ, Krestin GP. Stress myocardial perfusion: imaging with multidetector CT. Radiology. 2014 Jan;270(1):25-46.

27. Schelbert HR, Phelps ME, Huang SC, MacDonald NS, Hansen H, Selin C, et al. N-13 ammonia as an indicator of myocardial blood flow. Circulation. 1981 Jun;63(6):1259-72.

28. Tong CY, Prato FS, Wisenberg G, Lee TY, Carroll E, Sandler D, et al. Measurement of the extraction efficiency and distribution volume for Gd-DTPA in normal and diseased canine myocardium. Magn Reson Med. 1993 Sep;30(3):337-46.

29. Li X, Springer CS,Jr, Jerosch-Herold M. First-pass dynamic contrast-enhanced MRI with extravasating contrast reagent: evidence for human myocardial capillary recruitment in adenosine-induced hyperemia. NMR Biomed. 2009 Feb;22(2):148-57.

30. Ishida M, Ichihara T, Nagata M, Ishida N, Takase S, Kurita T, et al. Quantification of myocardial blood flow using model based analysis of first-pass perfusion MRI: extraction fraction of Gd-DTPA varies with myocardial blood flow in human myocardium. Magn Reson Med. 2011 Nov;66(5):1391-9.

31. Canty JM,Jr, Judd RM, Brody AS, Klocke FJ. First-pass entry of nonionic contrast agent into the myocardial extravascular space. Effects on radiographic estimates of transit time and blood volume. Circulation. 1991 Nov;84(5):2071-8.

32. Daghini E, Primak AN, Chade AR, Zhu X, Ritman EL, McCollough CH, et al. Evaluation of porcine myocardial microvascular permeability and fractional vascular volume using 64-slice helical computed tomography (CT). Invest Radiol. 2007 May;42(5):274-82.

33. Saraste A, Kajander S, Han C, Nesterov SV, Knuuti J. PET: Is myocardial flow quantification a clinical reality? J Nucl Cardiol. 2012 Oct;19(5):1044-59.

34. Sourbron SP, Buckley DL. Tracer kinetic modelling in MRI: estimating perfusion and capillary permeability. Phys Med Biol. 2012 Jan 21;57(2):R1-33.

35. Jerosch-Herold M, Swingen C, Seethamraju RT. Myocardial blood flow quantification with MRI by model-independent deconvolution. Med Phys. 2002 May;29(5):886-97.

36. Jerosch-Herold M, Wilke N, Stillman AE. Magnetic resonance quantification of the myocardial perfusion reserve with a Fermi function model for constrained deconvolution. Med Phys. 1998 Jan;25(1):73-84.

37. Broadbent DA, Biglands JD, Larghat A, Sourbron SP, Radjenovic A, Greenwood JP, et al. Myocardial blood flow at rest and stress measured with dynamic contrast-enhanced MRI: comparison of a distributed parameter model with a Fermi function model. Magn Reson Med. 2013 Dec;70(6):1591-7.

38. Johnson JA, Wilson TA. A model for capillary exchange. Am J Physiol. 1966 Jun;210(6):1299-303.

39. Koh TS, Cheong DL, Hou Z. Issues of discontinuity in the impulse residue function for deconvolution analysis of dynamic contrast-enhanced MRI data. Magn Reson Med. 2011 Sep;66(3):886-92.

40. Garpebring A, Ostlund N, Karlsson M. A novel estimation method for physiological parameters in dynamic contrast-enhanced MRI: application of a distributed parameter model using Fourier-domain calculations. IEEE Trans Med Imaging. 2009 Sep;28(9):1375-83.

41. St Lawrence KS, Lee TY. An adiabatic approximation to the tissue homogeneity model for water exchange in the brain: II. Experimental validation. J Cereb Blood Flow Metab. 1998 Dec;18(12):1378-85.

42. Bisdas S, Konstantinou G, Surlan-Popovic K, Khoshneviszadeh A, Baghi M, Vogl TJ, et al. Dynamic contrast-enhanced CT of head and neck tumors: comparison of first-pass and permeability perfusion measurements using two different commercially available tracer kinetics models. Acad Radiol. 2008 Dec;15(12):1580-9.

43. Goh V, Halligan S, Bartram CI. Quantitative tumor perfusion assessment with multidetector CT: are measurements from two commercial software packages interchangeable? Radiology. 2007 Mar;242(3):777-82.

44. So A, Hsieh J, Li JY, Hadway J, Kong HF, Lee TY. Quantitative myocardial perfusion measurement using CT perfusion: a validation study in a porcine model of reperfused acute myocardial infarction. Int J Cardiovasc Imaging. 2012 Jun;28(5):1237-48.

45. So A, Wisenberg G, Islam A, Amann J, Romano W, Brown J, et al. Non-invasive assessment of functionally relevant coronary artery stenoses with quantitative CT perfusion: preliminary clinical experiences. Eur Radiol. 2012 Jan;22(1):39-50.

46. Jerosch-Herold M, Wilke N, Wang Y, Gong GR, Mansoor AM, Huang H, et al. Direct comparison of an intravascular and an extracellular contrast agent for quantification of myocardial perfusion. Cardiac MRI Group. Int J Card Imaging. 1999 Dec;15(6):453-64.

47. Tofts PS, Brix G, Buckley DL, Evelhoch JL, Henderson E, Knopp MV, et al. Estimating kinetic parameters from dynamic contrast-enhanced T(1)-weighted MRI of a diffusable tracer: standardized quantities and symbols. J Magn Reson Imaging. 1999 Sep;10(3):223-32.

48. Pack NA, DiBella EV. Comparison of myocardial perfusion estimates from dynamic contrast-enhanced magnetic resonance imaging with four quantitative analysis methods. Magn Reson Med. 2010 Jul;64(1):125-37.

49. Sourbron SP, Buckley DL. On the scope and interpretation of the Tofts models for DCE-MRI. Magn Reson Med. 2011 Sep;66(3):735-45.

50. Patlak CS, Blasberg RG, Fenstermacher JD. Graphical evaluation of blood-to-brain transfer constants from multiple-time uptake data. J Cereb Blood Flow Metab. 1983 Mar;3(1):1-7.

51. Ichihara T, Ishida M, Kitagawa K, Ichikawa Y, Natsume T, Yamaki N, et al. Quantitative analysis of first-pass contrast-enhanced myocardial perfusion MRI using a Patlak plot method and blood saturation correction. Magn Reson Med. 2009 Aug;62(2):373-83.

52. Bamberg F, Hinkel R, Schwarz F, Sandner TA, Baloch E, Marcus R, et al. Accuracy of dynamic computed tomography adenosine stress myocardial perfusion imaging in estimating myocardial blood flow at various degrees of coronary artery stenosis using a porcine animal model. Invest Radiol. 2012 Jan;47(1):71-7.

53. Bamberg F, Klotz E, Flohr T, Becker A, Becker CR, Schmidt B, et al. Dynamic myocardial stress perfusion imaging using fast dual-source CT with alternating table positions: initial experience. Eur Radiol. 2010 May;20(5):1168-73.

54. Gould RG, Lipton MJ, McNamara MT, Sievers RE, Koshold S, Higgins CB. Measurement of regional myocardial blood flow in dogs by ultrafast CT. Invest Radiol. 1988 May;23(5):348-53.

55. Bindschadler M, Modgil D, Branch KR, La Riviere PJ, Alessio AM. Comparison of blood flow models and acquisitions for quantitative myocardial perfusion estimation from dynamic CT. Phys Med Biol. 2014 Apr 7;59(7):1533-56.

56. Muehling OM, Wilke NM, Panse P, Jerosch-Herold M, Wilson BV, Wilson RF, et al. Reduced myocardial perfusion reserve and transmural perfusion gradient in heart transplant arteriopathy assessed by magnetic resonance imaging. J Am Coll Cardiol. 2003 Sep 17;42(6):1054-60.

57. Christian TF, Aletras AH, Arai AE. Estimation of absolute myocardial blood flow during first-pass MR perfusion imaging using a dual-bolus injection technique: comparison to single-bolus injection method. J Magn Reson Imaging. 2008 Jun;27(6):1271-7.

58. Christian TF, Rettmann DW, Aletras AH, Liao SL, Taylor JL, Balaban RS, et al. Absolute myocardial perfusion in canines measured by using dual-bolus first-pass MR imaging. Radiology. 2004 Sep;232(3):677-84.

59. Hsu LY, Groves DW, Aletras AH, Kellman P, Arai AE. A quantitative pixel-wise measurement of myocardial blood flow by contrast-enhanced first-pass CMR perfusion imaging: microsphere validation in dogs and feasibility study in humans. JACC Cardiovasc Imaging. 2012 Feb;5(2):154-66.

60. Miller CA, Naish JH, Ainslie MP, Tonge C, Tout D, Arumugam P, et al. Voxel-wise quantification of myocardial blood flow with cardiovascular magnetic resonance: effect of variations in methodology and validation with positron

emission tomography. J Cardiovasc Magn Reson. 2014 Jan 24;16:11,429X-16-11.

61. Pack NA, DiBella EV, Rust TC, Kadrmas DJ, McGann CJ, Butterfield R, et al. Estimating myocardial perfusion from dynamic contrast-enhanced CMR with a model-independent deconvolution method. J Cardiovasc Magn Reson. 2008 Nov 12;10:52,429X-10-52.

62. Henderson E, Rutt BK, Lee TY. Temporal sampling requirements for the tracer kinetics modeling of breast disease. Magn Reson Imaging. 1998 Nov;16(9):1057-73.

63. Gebker R, Jahnke C, Paetsch I, Schnackenburg B, Kozerke S, Bornstedt A, et al. MR myocardial perfusion imaging with k-space and time broad-use linear acquisition speed-up technique: feasibility study. Radiology. 2007 Dec;245(3):863-71.

64. Spira D, Gerlach JD, Spira SM, Schulze M, Sauter A, Horger M. Effect of scan time on perfusion and flow extraction product (K-trans) measurements in lung cancer using low-dose volume perfusion CT (VPCT). Acad Radiol. 2012 Jan;19(1):78-83.

65. Ng CS, Chandler AG, Wei W, Anderson EF, Herron DH, Kurzrock R, et al. Effect of sampling frequency on perfusion values in perfusion CT of lung tumors. AJR Am J Roentgenol. 2013 Feb;200(2):W155-62.

66. Goh V, Liaw J, Bartram CI, Halligan S. Effect of temporal interval between scan acquisitions on quantitative vascular parameters in colorectal cancer: implications for helical volumetric perfusion CT techniques. AJR Am J Roentgenol. 2008 Dec;191(6):W288-92.

67. Cao Y, Li D, Shen Z, Normolle D. Sensitivity of quantitative metrics derived from DCE MRI and a pharmacokinetic model to image quality and acquisition parameters. Acad Radiol. 2010 Apr;17(4):468-78.

68. Kershaw LE, Cheng HL. Temporal resolution and SNR requirements for accurate DCE-MRI data analysis using the AATH model. Magn Reson Med. 2010 Dec;64(6):1772-80.

69. Fujita M, Kitagawa K, Ito T, Shiraishi Y, Kurobe Y, Nagata M, et al. Dose reduction in dynamic CT stress myocardial perfusion imaging: comparison of 80-kV/370-mAs and 100-kV/300-mAs protocols. Eur Radiol. 2014 Mar;24(3):748-55.

70. Schwab F, Ingrisch M, Marcus R, Bamberg F, Hildebrandt K, Adrion C, et al. Tracer kinetic modeling in myocardial perfusion quantification using MRI. Magn Reson Med. 2015 Mar;73(3):1206-15.

71. Czernin J, Muller P, Chan S, Brunken RC, Porenta G, Krivokapich J, et al. Influence of age and hemodynamics on myocardial blood flow and flow reserve. Circulation. 1993 Jul;88(1):62-9.

72. Sdringola S, Johnson NP, Kirkeeide RL, Cid E, Gould KL. Impact of unexpected factors on quantitative myocardial perfusion and coronary flow reserve in young, asymptomatic volunteers. JACC Cardiovasc Imaging. 2011 Apr;4(4):402-12.

73. Nakamori S, Onishi K, Ishida M, Nakajima H, Yamada T, Nagata M, et al. Myocardial perfusion reserve is impaired in patients with chronic obstructive pulmonary disease: a comparison to current smokers. Eur Heart J Cardiovasc Imaging. 2014 Feb;15(2):180-8.

74. Nakajima H, Onishi K, Kurita T, Ishida M, Nagata M, Kitagawa K, et al. Hypertension impairs myocardial blood perfusion reserve in subjects without regional myocardial ischemia. Hypertens Res. 2010 Nov;33(11):1144-9.

75. Kawecka-Jaszcz K, Czarnecka D, Olszanecka A, Klecha A, Kwiecien-Sobstel A, Stolarz-Skrzypek K, et al. Myocardial perfusion in hypertensive patients with normal coronary angiograms. J Hypertens. 2008 Aug;26(8):1686-94.

507555-L-bw-Pelgrim
Processed on: 26-1-2017

III

Static CT perfusion experiments

507555-L-bw-Pelgrim
Processed on: 26-1-2017

507555-L-bw-Pelgrim
Processed on: 26-1-2017